Study and Comparison of Discontinuous Modulation for Modular Multilevel Converters in Motor Drive Applications

Ricard Picas, Jordi Zaragoza, *Member, IEEE,* Josep Pou, *Fellow, IEEE,*
Salvador Ceballos, Georgios Konstantinou, *Senior Member, IEEE,* and Gabriel J. Capella

***Abstract*—Discontinuous modulation applied to modular multilevel converters is an effective method for reducing the capacitor voltage ripples. In this paper, the discontinuous modulation is adapted and used in a motor drive application. For proper operation of the converter, a new energy controller is presented, which is suitable for operation with non-sinusoidal reference signals. Experimental results comparing the discontinuous modulation with other techniques operating at low motor speeds are shown. The results demonstrate the effectiveness of the discontinuous modulation on reducing capacitor voltage ripples and power losses.**

***Index Terms*—Modular multilevel converter, discontinuous modulation, motor drive, low frequency operation.**

I. Introduction

MULTILEVEL converters are power converter topologies suitable for medium- and high-power applications [1], [2]. Among the multilevel converter topologies, the modular multilevel converter (MMC) [3]–[5] has become the most attractive topology for high-voltage direct current (HVDC) transmission systems [6] and flexible alternating current transmission systems (FACTS) [7]. The most attractive features of the MMC are [4]: (i) its modularity and scalability to different power and voltage levels, (ii) its high efficiency, (iii) the high quality of the output voltages, and (iv) the absence of additional capacitors on the dc-link, as the storage is distributed among the capacitors in the submodules (SMs) of the converter.

In the field of high-power motor drives (megawatt range), the quality of the voltages generated by the power converter is a decisive factor. Voltage harmonics cause additional power losses to the motor that reduce its efficiency and complicates thermal management, this is why the MMC is a promising topology in this field. Suitability of the MMC in the area of medium-voltage motor drives has also been reported [8], [9]. However, the main challenge that limits the wide-spread use of the MMC in motor drive applications is the large capacitor voltage ripples produced under low speed operation. The capacitor voltage ripple amplitudes are inversely proportional to the output frequency of the converter, i.e. the motor speed.

Multiple solutions have been proposed to reduce the capacitor voltage ripples in motor-drive applications. Some publications propose the use of new MMC topologies [10]–[13] or MMCs based on full-bridge sub-modules (SMs) [14], [15]. However, reducing capacitor voltage ripples using the standard MMC topology based on half-bridge SMs remains a challenge.

Controlling the circulating current to reduce the capacitor voltage ripples has been extensively studied [16]–[18]. However, when operating with low frequencies, those techniques cannot reduce the capacitor voltage ripples enough. Some recent techniques allow the MMC to operate in the low frequency range [19], [20]. Operation of the MMC at very low frequencies was firstly achieved in [21], where a sinusoidal zero-sequence component of a higher frequency was added to the modulation signals in combination with circulating currents of the same frequency. This technique is able to shift the power fluctuations to a higher frequency, achieving a significant reduction in the capacitor voltage ripples. It is only practical when operating with low output frequencies, otherwise the frequency of the injected zero-sequence component would be excessively high. For this reason, [22] and [23] present hybrid mechanisms that switch from low to high speed operation modes. In the case of high speed operation, the average SM capacitor voltages can be reduced to accommodate higher voltage ripples [24].

With the objective of reducing the circulating current and conduction power losses, a technique based on the injection of a square-wave zero-sequence signal and a square-wave circulating current is presented in [25]. This technique achieves a reduction of up to a 50% of the circulating current peak value. Similar techniques are presented in [26] and [27], which combine the square-wave zero-sequence with a sinusoidal circulating current.

Discontinuous modulation is another technique that can be used for reducing the capacitor voltage ripples [28], [29].

This work was supported by the Ministerio de Economía y Competitividad of Spain under Project ENE2012-36871-C02-00, partially funded by the European Union and Secretaria d'Universitats i Recerca del Departament d'Empresa i Coneixement de la Generalitat de Catalunya.

R. Picas is with Ingenia Motion Control, 08042 Barcelona, Spain (e-mail: rpicas@ingeniamc.com).

J. Zaragoza and G. J. Capella are with the Terrassa Industrial Electronics Group, Technical University of Catalonia, 08222 Barcelona, Spain (e-mails: jordi.zaragoza-bertomeu@upc.edu, gabriel.jose.capella@upc.edu)

J. Pou is with the School of Electrical and Electronic Engineering, Nanyang Technology University, 639798 Singapore (e-mail: j.pou@ntu.edu.sg).

S. Ceballos is with the Energy Unit, Tecnalia Research and Innovation, 48160 Derio, Spain (e-mail:salvador.ceballos@tecnalia.com).

G. Konstantinou is with the School of Electrical Engineering and Telecommunications, UNSW Sydney, Sydney, NSW, 2052 Australia (e-mail:g.konstantinou@unsw.edu.au)

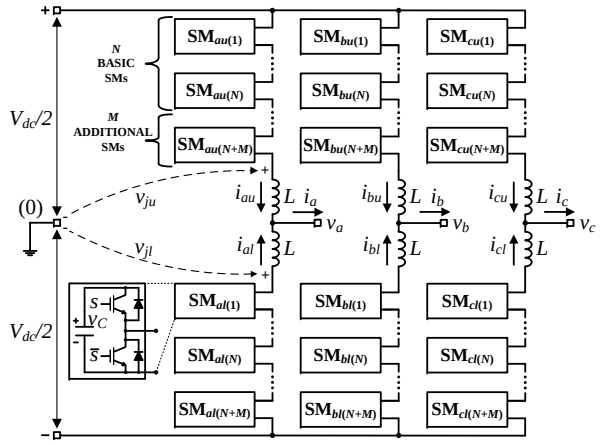

Fig. 1. Circuit diagram of a three-phase MMC with N basic SMs and M additional SMs per arm.

Through the addition of a zero-sequence to the modulation signal, this technique clamps one arm of the converter to a non-switching position. Combined with the injection of a circulating current, most of the output current flows through the arm where no SMs are activated, hence achieving a significant reduction in the capacitor voltage ripples. Moreover, clamping the arms in a non-switching position reduces the switching power losses.

Effectiveness of discontinuous modulation has been demonstrated in grid-frequency applications, but it has never been tested in variable-speed motor drives. In this paper, the discontinuous modulation technique is applied to a motor drive based on a permanent-magnet synchronous machine (PMSM). The modulation technique has been implemented together with a typical field-oriented control (FOC) technique. The common energy balancing controllers based on the injection of a fundamental component, as in [18], [30], do not present an optimal performance with this modulation technique. Therefore, a new energy controller based on the instantaneous values of the reference signals is also proposed. Such a controller is here refered to as modulated energy controller.

Ultra-low frequency operation of the converter with discontinuous modulation has been demonstrated, driving a PMSM at a speed of 30 r/min (1% of the nominal value) with a load torque of 70%. In order to highlight the benefits of this technique, the results have been compared with those achieved using the techniques based on sinusoidal [21] and square-wave [25] zero-sequence signal injection. The discontinuous modulation produces capacitor voltage ripples similar to those obtained with the injection of a higher frequency signal in the zero-sequence and the circulating currents, but can achieve a significant reduction in the rms value of the circulating currents and, hence, in the power losses.

The rest of this paper is organized as follows. Section II summarizes the principles of operation and the implementation of the discontinuous modulation in the MMC. Section III presents the control scheme of the motor drive and demonstrates the implementation of the modulated energy controller. Section IV deals with the equations of the sinusoidal and square-wave techniques used for benchmarking and presents experimental results. Finally, Section V summarizes the main conclusions of this work.

II. MMC and Discontinuous Modulation

A. MMC Fundamentals

The MMC consists of two arms per phase-leg, where each arm comprises N series-connected, identical SMs and a series arm inductor (L). Each SM contains a half-bridge circuit and a capacitor C. The output voltage of each SM equals its capacitor voltage (v_C) when the SM is activated, or equals zero when it is deactivated. A schematic of the topology is depicted in Fig. 1. In this figure, in addition to the N basic SMs of each arm, M additional SMs have been included. These additional SMs are needed when operating the MMC with the discontinuous modulation.

The currents that flow through the upper and lower arms, i_{ju} and i_{jl} for $j = \{a, b, c\}$, respectively, are composed by half of the output current and a circulating current:

$$i_{ju} = \frac{i_j}{2} + i_{j\,\text{circ}} \qquad \text{and} \qquad i_{jl} = \frac{i_j}{2} - i_{j\,\text{circ}}\,. \tag{1}$$

The circulating current includes a dc component, related with the power exchange between the dc and ac sides of the converter, and some harmonic components. In order to improve the converter dynamics and reduce the capacitor voltage ripples, the circulating current should be controlled.

B. Discontinuous Modulation. Principles of Operation

The discontinuous pulse-width modulation (DPWM) consists in adding a zero-sequence signal to the reference signals of a multiphase converter [31]. The injected zero-sequence is such that one of the phase-legs is clamped either to the upper or to the lower terminals of the dc-link for certain time intervals [29]. This implementation can considerably reduce the power losses for high modulation indices and, in a more moderate way, for low modulation indices. In cases of low-speed motor drive applications, the number of SMs per arm should be kept as small as possible in order not to increase the power losses produced on account of the large transitions needed for clamping the arm voltage under such conditions [29]. Besides, DPWM can reduce the SM capacitor voltage ripple, especially for low modulation indices [29]. The dynamic model of the MMC presented in [18] demonstrates that, ideally, the arm that has fewer activated SMs is the one that carries more output current. Therefore, when one of the arms of a phase-leg is clamped to a dc-link terminal, the clamped arm provides all the output current, while no current circulates through the unclamped arm of that phase-leg. This effect can be seen in the equations of the ideal arm currents, where a modulation reference signal of 1 or -1 produces no current in either the lower or the upper arm, respectively [18]:

$$i_{ju} = i_j \frac{1 + v_{jm}}{2} \quad \text{and} \quad i_{jl} = i_j \frac{1 - v_{jm}}{2}\,, \tag{2}$$

where v_{jm} is the normalized reference signal, which can vary within the [-1,1] range, under linear operation mode.

Consequently, no current circulates through any SM capacitor of the whole phase-leg and hence the overall capacitor

voltage ripples are reduced. From (2), the ideal reference for the circulating current is:

$$i^*_{j\ \text{circ}} = \frac{i_{ju} - i_{jl}}{2} = \frac{i_j v_{jm}}{2} \ . \tag{3}$$

The reduction in the capacitor voltage ripples is more significant when operating with low modulation indices. This is because when no zero-sequence is injected, a similar number of SMs are activated in both arms. Under such operating conditions, the output current is rather evenly shared between both arms of a phase-leg, flowing through N SMs and producing large capacitor voltage deviations. However, if discontinuous modulation is implemented, the zero-sequence shifts the reference signals of all the phases far from zero, reducing the currents in the capacitors and, hence, the capacitor voltage ripples.

In order to improve the performance of the modulation technique, the clamping intervals are selected by a closed-loop algorithm [29]. At each sampling period, two phase-legs can be clamped: the one with the highest voltage reference and the one with the lowest voltage reference. In order to further reduce the switching power losses and capacitor voltage ripples, the arm with the highest absolute value of its output current is the selected one to be clamped.

C. Control of the Circulating Current in Discontinuous Modulation

The circulating current is controlled by adding a differential control signal Δv_{jm} to the common modulation signal, as follows:

$$v_{jum} = v_{jm} + \Delta v_{jm} \qquad \text{and} \qquad v_{jlm} = v_{jm} - \Delta v_{jm} \tag{4}$$

where v_{jum} and v_{jlm} are the reference signals for the upper and lower arms, respectively.

Once the differential control signal is added, the zero-sequence signal (v_{zs}) of the discontinuous modulation is calculated as the difference between the clamping level (1 or -1) and the reference signal of the arm which has been selected by the closed-loop algorithm [29]. The zero-sequence signal is calculated as

$$v_{zs} = 1 - v_{jum} \qquad \text{or} \qquad v_{zs} = -1 - v_{jlm} \ , \tag{5}$$

when clamping the upper or lower arm, respectively. Then, this zero-sequence is added to the reference signals for the six arms, obtaining the discontinuous modulation references for the upper and lower arms (v_{jud} and v_{jld}):

$$v_{jud} = v_{jum} + v_{zs} \qquad \text{and} \qquad v_{jld} = v_{jlm} + v_{zs} \ . \tag{6}$$

If the differential control signal (Δv_{jm}) of the clamped arm is positive, then the reference of the upper arm is higher than the reference of the lower arm and, therefore, all the modulation signals remain within the modulation limits [-1,1]. However, if the differential control signal is negative, then the reference of the arm which is opposite to the clamped one, presents a value that is either higher than 1 or lower than -1. In order to maintain control of the circulating current during the clamping periods, this over-modulation situation has to be avoided.

The addition of M SMs to the N basic ones of each arm [29] extends the modulation range beyond the interval [-1,1], and thus allows for controlling the circulating current during the intervals where the phase-leg is clamped. The addition of SMs in the arms increases the cost of the MMC, but also provides extra benefits to the converter, such as fault tolerance capability and a further reduction in the capacitor voltage ripples [32]. Another possible solution consists on implementing an alternative discontinuous modulation technique [33], which does not require the use of additional SMs. Although this second solution does not increase the cost of the converter, the reduction of the capacitor voltage ripples (the main objective in this application) is not as efficient. It also produces more switching power losses because of the fact that the arm that should be clamped has to be unclamped for some intervals in order to be able to control the circulating current. Besides, the addition of SMs to the arm enables the converter for fault tolerant operation. Since one of the objectives of this paper is the comparison of DPWM with other low-speed techniques, the additional SMs have been used in all the cases, providing the same benefits and drawbacks to all of them.

D. Capacitor Voltage Variation with DPWM

Although the zero-sequence signal is calculated in a closed-loop algorithm, the clamping periods can be deduced when considering ideal performance of the converter. That is, considering that the output currents are purely sinusoidal and that the differential control signal can be neglected. For the sake of simplification, the current is also assumed to be in phase with the reference voltage. Under such conditions, the six clamping intervals can be defined and the zero-sequence signal calculated:

$$v_{zs} = \begin{cases} 1 - m\,\cos(\omega t) & \text{if } -\frac{\pi}{6} < \omega t < \frac{\pi}{6} \\ -1 - m\,\cos\left(\omega t + \frac{2\pi}{3}\right) & \text{if } \frac{\pi}{6} < \omega t < \frac{3\pi}{6} \\ 1 - m\,\cos\left(\omega t - \frac{2\pi}{3}\right) & \text{if } \frac{3\pi}{6} < \omega t < \frac{5\pi}{6} \\ -1 - m\,\cos(\omega t) & \text{if } \frac{5\pi}{6} < \omega t < \frac{7\pi}{6} \\ 1 - m\,\cos\left(\omega t + \frac{2\pi}{3}\right) & \text{if } \frac{7\pi}{6} < \omega t < \frac{9\pi}{6} \\ -1 - m\,\cos\left(\omega t - \frac{2\pi}{3}\right) & \text{if } \frac{9\pi}{6} < \omega t < \frac{11\pi}{6} \end{cases} \tag{7}$$

Once the zero-sequence signal is known, and considering the dynamic model of the converter [34], the voltage of the upper arm SM capacitors of phase a can be calculated as:

$$v_{Cau} = \frac{1}{C}\int_0^t i_{au}\frac{1 - v_{aud}}{2}dt \ . \tag{8}$$

From (6), (7) and (8), the piece-wise defined function of the voltage variation (9) is calculated. In (9), I_a is the amplitude of the output current and V_{C0} is the final voltage in the previous clamping period.

Considering that in a motor drive application the output voltage (and the modulation index) is proportional to the output frequency, the common term $\frac{3I_a m}{8\omega C}$ in (9) can be considered constant. This means that the capacitor voltage ripple amplitude is no longer inversely proportional to the

$$v_{Cau} = \begin{cases} V_{C0} & \text{if } -\frac{\pi}{6} < \omega t < \frac{\pi}{6} \text{ or} \\ & \text{if } \frac{5\pi}{6} < \omega t < \frac{7\pi}{6} \\ V_{C0} + \frac{3I_a m}{8\omega C} \left\{ \left[\left(\omega t - \frac{1}{\sqrt{3}} \cos\left(2\omega t + \frac{\pi}{3}\right) \right) \right] \cdot (-1)^x \right. & \\ \left. + m \left[\frac{\sqrt{7}}{2} \sin\left(\omega t + \pi - \frac{1}{3}\right) + \frac{1}{6} \sin\left(3\omega t + \frac{2\pi}{3}\right) \right] \right\} & \text{if } \frac{\pi}{6} < \omega t < \frac{3\pi}{6}; \quad x = 0 \\ & \text{if } \frac{7\pi}{6} < \omega t < \frac{9\pi}{6}; \quad x = 1 \\ V_{C0} + \frac{3I_a m}{8\omega C} \left\{ \left[\left(\omega t + \frac{1}{\sqrt{3}} \cos\left(2\omega t - \frac{\pi}{3}\right) \right) \right] \cdot (-1)^x \right. & \\ \left. + m \left[\frac{\sqrt{7}}{2} \sin\left(\omega t + \pi + \frac{1}{3}\right) + \frac{1}{6} \sin\left(3\omega t + \frac{2\pi}{3}\right) \right] \right\} & \text{if } \frac{3\pi}{6} < \omega t < \frac{5\pi}{6}; \quad x = 1 \\ & \text{if } \frac{9\pi}{6} < \omega t < \frac{11\pi}{6}; \quad x = 0. \end{cases} \tag{9}$$

output frequency, allowing the converter to operate at low speeds.

Moreover, (9) demonstrates that the voltage variation in the capacitors is bounded and, therefore, the maximum and minimum values can be found. Two main terms can be identified in (9); a first one which is independent of the modulation index, and a second one which is proportional to the modulation index:

$$\Delta v_{C\ \text{DPWM min (m=1)}} = \frac{I_a}{4\omega_N C} \cdot 0.6416 \text{ and} \tag{10}$$

$$\Delta v_{C\ \text{DPWM max}(m\to 0)} = \frac{I_a}{4\omega_N C} \cdot \pi\ , \tag{11}$$

where ω_N is the nominal speed of the motor. As a consequence, the minimum capacitor voltage ripple happens with a modulation index equal to 1 and the maximum ripple is produced when the modulation index tends towards 0.

On the contrary, a sinusoidal modulation will produce a voltage variation inversely proportional to the fundamental frequency, tending to infinite when the modulation frequency tends to zero. In order to illustrate this fact, the voltage variation with a purely sinusoidal modulation index and the capacitor voltage ripples at modulation index equal to 1 and to 0.1 have been obtained:

$$v_{C\ \text{SPWM}} = \frac{I_a}{4\omega C} \left[\sin(\omega t) - \frac{m^2}{4} \left(\sin(\omega t) + \frac{1}{3} \sin(3\omega t) \right) \right] , \tag{12}$$

$$\Delta v_{C\ \text{SPWM}\ min(m=1)} = \frac{I_a}{4\omega_N C} \cdot \frac{2}{3} \quad \text{and} \tag{13}$$

$$\Delta v_{C\ \text{SPWM}\ (m=0.1)} = \frac{I_a}{4\omega_N C} \cdot 9.935\ . \tag{14}$$

The theoretical capacitor voltage ripples at a modulation index equal to 1 are very similar, albeit slightly smaller with DPWM. However, since the voltage ripples with sinusoidal modulation are inversely proportional to the output frequency, when the modulation index is 0.1 (10% of nominal speed), the voltage ripples are more than three times larger than those obtained with DPWM.

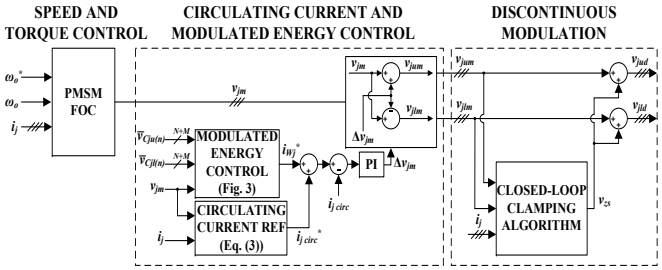

Fig. 2. Block diagram of the control scheme.

III. Control Scheme

The control scheme proposed in this paper can be divided into three main blocks. The first one is the FOC that consists of the PMSM speed and torque control loops. The second block is composed of the circulating current controller and the modulated energy controller, which produces a signal to be added to the circulating current reference. Finally, the discontinuous modulation block which calculates and adds the zero-sequence component. A block diagram of the total control scheme is depicted in Fig. 2.

In order to determine the output voltage level, either phase-shifted PWM (PS-PWM) or level-shifted PWM (LS-PWM) techniques can be used in such an application. In terms of capacitor voltage ripple, PS-PWM and LS-PWM show some differences [35]. However, for low modulation indices, which are usually required in motor drive applications, such differences are not relevant [29]. Phase-disposition PWM (PD-PWM) shows better line-to-line voltages when compared to PS-PWM in terms of total harmonic distortion (THD) and weighted total harmonic distortion WTHD [36]. Once the final modulation signals are calculated, the output voltage level is obtained from a PD-PWM stage and the SMs to be activated are selected by means of a voltage balancing algorithm [37].

A. PMSM FOC

A standard FOC strategy [38] is implemented. It is based on the d-q model of the PMSM:

$$v_d = R_s i_d + L_d \frac{d}{dt} i_d - \omega_e L_q i_q \quad \text{and} \tag{15}$$

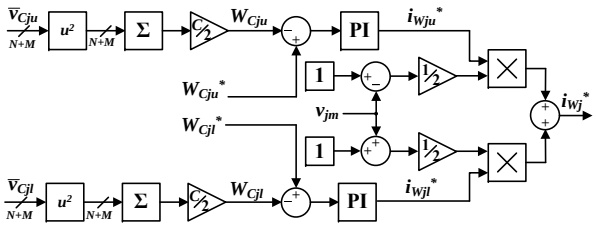

Fig. 3. Block diagram of the proposed modulated energy control (MEC).

$$v_q = R_s i_q + L_q \frac{d}{dt} i_q + \omega_e L_d i_d + \omega_e \lambda_m \ , \qquad (16)$$

where v_d and v_q are the stator voltage components, i_d and i_q are the stator current components, R_s is the stator resistance, L_d and L_q are the equivalent d-q inductances, λ_m is the magnetic flux of the permanent magnets, and ω_e is the electrical frequency. The electrical frequency is calculated as a product of the mechanical speed ω_o and the number of pole pairs of the machine (p).

B. Circulating Current and Modulated Energy Controllers

The second control block consists of the circulating current controller and the voltage reference calculation. As introduced in Subsection II-B, the circulating current is controlled trough the differential control signal Δv_{jm}. This control variable is added to and subtracted from the common reference signal according to (4), thus creating two different reference signals, one for the upper arm and another one for the lower arm (v_{jum} and v_{jlm}, respectively). The differential control signal is calculated through a PI controller.

The main reference for the circulating current is given by (3). An additional component to achieve energy balance between the upper and lower arms needs to be added to the circulating current reference. The implementation of an energy balancing controller based on the injection of a fundamental component was presented in [30]. This technique is based on the energy transfer that happens when multiplying a sinusoidal arm voltage by a sinusoidal differential current with the same phase. However, when the main component of the inner arm voltage is not the fundamental component, as it happens in discontinuous modulation when operating with low modulation indices, a sinusoidal current is not the optimal reference for balancing the energy between the arms.

For this reason, this paper proposes a new energy control technique, named modulated energy control (MEC), which is adaptable to all kinds of modulation signals. In the MEC technique, two control loops are implemented, one per each arm. Each control loop regulates the energy stored in the upper (W_{Cju}) or lower (W_{Cjl}) arms individually, defining two different current references (i^*_{Wju} and i^*_{Wjl}). Then, those references are applied proportionally to the inner voltage, calculating two arm references and adding them to the main ones. The total energy control current reference is defined as:

$$i^*_{Wj} = i^*_{Wju} \frac{1 - v_{jm}}{2} + i^*_{Wjl} \frac{1 + v_{jm}}{2} \ . \qquad (17)$$

This weighting process applies the current references proportionally to the number of SMs activated in each arm,

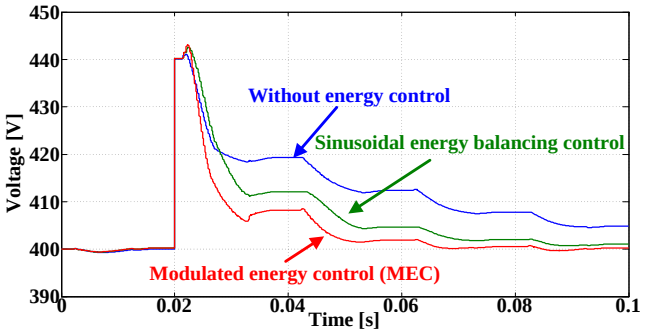

Fig. 4. Simulation results. Upper arm capacitor voltage when a voltage imbalance is applied. Comparison of the MEC with the traditional sinusoidal energy balancing technique and without any energy controller.

hence improving the energy control. As an example, when the modulation signal is 1, and hence no SMs are activated in the upper arm, the energy control current reference for that arm is multiplied by zero, since this reference would have no effect on the capacitor voltages. On the contrary, the energy control current reference for the lower arm is multiplied by one, since all the SMs in that arm are activated and it has the maximum effect.

The MEC not only regulates the energy balance between upper and lower arms, but also the average energy stored in each arm. The average control is performed because the current references are not calculated from the energy difference between the arms, but from the error between the energy reference and the measured arm energy. A block diagram of the proposed MEC is depicted in Fig. 3.

Simulation results using a MATLAB/Simulink model of the MMC with 4 SMs per arm ($N = 3$ and $M = 1$) have been obtained to demonstrate the effectiveness of the new energy control technique. In order to reduce the duration of the transient and non-ideal effects, the results have been obtained with higher voltage values ($V_{dc} = 1200$ V) and operating with an R-L load (10 Ω and 3 mH).

Fig. 4 shows the capacitor voltages of the upper arm when applying different control strategies: without energy balancing control, with a sinusoidal energy balancing control, and with the proposed MEC. In the three cases, an initial voltage imbalance of 10% is applied at $t = 0.2$ s. DPWM is applied with a sinusoidal reference signal of frequency 50 Hz and $m = 0.1$. Fig. 4 demonstrates that the proposed technique balances the SM voltages faster than the other techniques.

C. Discontinuous Modulation

The third block calculates and adds the discontinuous zero-sequence signal to the reference signals for the upper and lower arms [29]. The six reference signals, i.e. two for each phase-leg, and the three output current measurements are used to select the arm to be clamped. The arms that are candidates to be clamped are, amongst the upper arms, the one with the highest reference signal and, amongst the lower arms, the one with the lowest reference signal. In order to reduce switching power losses, the ultimately chosen arm is the one that belongs

TABLE I
SPECIFICATIONS OF THE PMSM

Parameter	Value
Output Power, P	200 W
Rated Current, I	2 A
Rated Torque, T_e	0.64 Nm
Rated Speed, ω_o	3000 r/min
Pole Pairs, p	4
Stator Inductors, L_d and L_q	8.45 mH
Stator Resistance, R_s	2.5 Ω
Magnet Flux, λ_m	0.045 Wb

to the phase-leg carrying the highest absolute value of the output current.

IV. EXPERIMENTAL RESULTS

The proposed modulation technique has been implemented and tested on a low-power laboratory prototype. The system consists of a three-phase MMC driving a PMSM. Each arm is composed of four SMs: three basic ones ($N = 3$) and an additional one ($M = 1$). The dc-link voltage is 120 V, the SM capacitors are of 1500 μF and the arm inductance is equal to 3mH. The converter has been implemented using silicon-carbide (SiC) technology, with MOSFET devices CREE CM-F20120D and Schottky diodes CREE C4D10120D. The motor is a 200-W PMSM Yaskawa Servomotor 02CE2 (Table I), and the main control and acquisition tasks are implemented on a dSPACE DS1006 with two high-speed analog-to-digital boards and an FPGA board. A picture of the experimental prototype is presented in Fig. 5.

All experiments are conducted with a 5 kHz switching frequency for the MMC and with a constant torque load of 70% of the rated torque and at speeds of 1500 r/min, 120 r/min and 30 r/min, which represent 50%, 4% and 1% of the rated speed, respectively.

A. Benchmarking Techniques

Experimental results have been obtained with discontinuous modulation (DPWM) and compared with carrier-based space-vector PWM (CB-SVPWM), consisting of sinusoidal modulation with zero-sequence injection based on space-vector modulation (SVM) [31]. The results obtained with DPWM have also been compared with two state-of-the-art techniques for low-speed operation, used for benchmarking. The benchmarking techniques are the one based on the injection of a sinusoidal zero-sequence component and a sinusoidal circulating current [21], hereinafter called CMsin, and the one based on the injection of a square-wave zero-sequence component and a square-wave circulating current [25], hereinafter called CMsqr.

In all three techniques, i.e. CB-SVPWM, CMsin and CMsqr, the common-mode component is added to the voltage references and included in the calculation of the circulating current reference. All techniques are implemented with the modulated energy controller. In CB-SVPWM, the circulating current reference is calculated using (3), while the zero-sequence is based on SVM patterns [31]:

$$v_{zs\,\mathrm{SVM}} = -\frac{\max\{v_{as}, v_{bs}, v_{cs}\} + \min\{v_{as}, v_{bs}, v_{cs}\}}{2}. \quad (18)$$

The CMsin modulation contains a sinusoidal zero-sequence component with amplitude $U_{\sin}$ and angular frequency $\omega_{\sin}$. The amplitude has to be large enough to reduce the capacitor voltage ripples and minimize the circulating currents, which are inversely proportional to the zero-sequence voltage amplitude. However, the amplitude of the zero sequence is limited by the modulation range. The values of $U_{\sin}$ and $f_{\sin}$ ($f_{\sin} = \omega_{\sin}/2\pi$) used in the experimental results are 40 V and 50 Hz, respectively. The zero-sequence voltage and the circulating current reference used in CMsin are:

$$v_{\sin} = U_{\sin}\sin(\omega_{\sin} t) \quad \text{and} \quad (19)$$

$$i^*_{j\,\mathrm{circ\,sin}} = \frac{2v_{js}^2/V_{dc} - V_{dc}/2}{U_{\sin}} i_j \sin(\omega_{\sin} t)\,. \quad (20)$$

The CMsqr is based on a square-wave zero-sequence signal and has the advantage of requiring lower circulating currents for the same zero-sequence amplitude. The amplitude U_{sqr} and frequency f_{sqr} have been chosen to be the same as in CMsin. The zero-sequence voltage and the circulating current in CMsqr are:

$$v_{\mathrm{sqr}} = \begin{cases} -U_{\mathrm{sqr}} & \text{if } 0 < t < \dfrac{1}{2f_{\mathrm{sqr}}} \\ U_{\mathrm{sqr}} & \text{if } \dfrac{1}{2f_{\mathrm{sqr}}} < t < \dfrac{1}{f_{\mathrm{sqr}}} \end{cases} \quad \text{and} \quad (21)$$

$$i^*_{\mathrm{j\,circ\,sqr}} = \begin{cases} -\dfrac{\dfrac{2v_{js}^2}{V_{dc}} - \dfrac{V_{dc}}{2}}{2U_{\mathrm{sqr}}} i_j & \text{if } 0 < t < \dfrac{1}{2f_{\mathrm{sqr}}} \\ \dfrac{\dfrac{2v_{js}^2}{V_{dc}} - \dfrac{V_{dc}}{2}}{2U_{\mathrm{sqr}}} i_j & \text{if } \dfrac{1}{2f_{\mathrm{sqr}}} < t < \dfrac{1}{f_{\mathrm{sqr}}} \end{cases}. \quad (22)$$

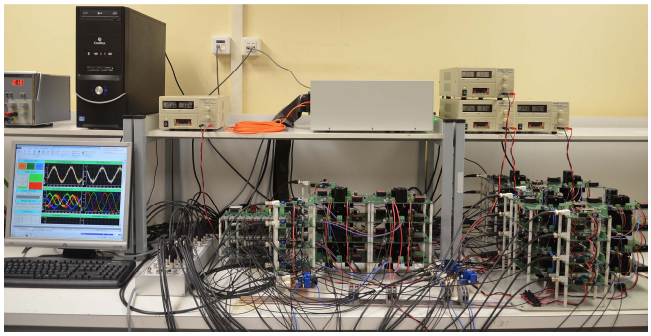

Fig. 5. Three-phase MMC laboratory prototype with four SMs per arm ($N = 3$ and $M = 1$).

B. Minimum Speed with CB-SVPWM

In Fig. 6, experimental results driving a motor at 120 r/min with load of 70% of rated torque (equivalent to an rms current of 1.4 A) are presented. Phase-a upper arm capacitor voltages for several operating modes are shown. It can be seen that

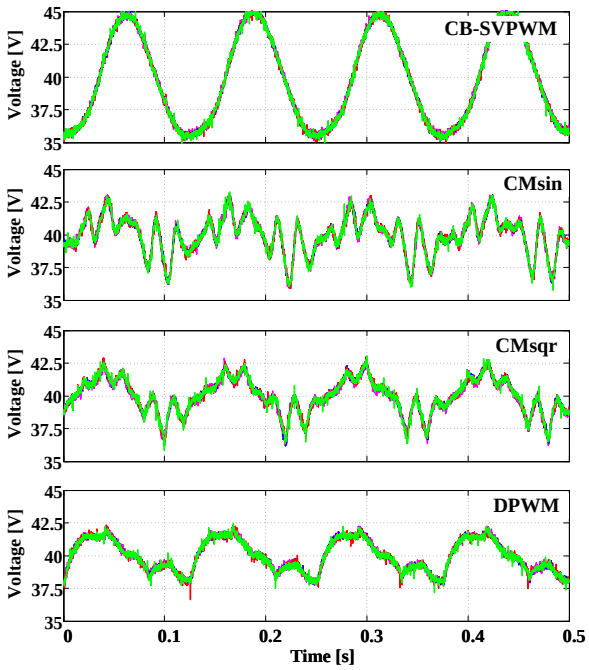

Fig. 6. Experimental results at the minimum speed achieved by CB-SVPWM (120 r/min). SM capacitor voltages.

with CB-SVPWM the peak-to-peak voltage is 10 V, which is 25% of the average voltage ($V_{Cavg} = 40V$). This is the minimum speed that can be achieved with this modulation technique, since lower speeds produce excessive capacitor voltage ripples that cause instability. When using CMsin and CMsqr, the capacitor voltage ripples are lower, having a peak-to-peak value of 6 V with CMsin and of 5 V with CMsqr. The peak-to-peak capacitor voltage obtained with DPWM is slightly smaller than that produced with CMsqr.

C. Operation at Very Low Speed

In order to highlight the advantages of DPWM, the capacitor voltage ripples and circulating currents at very low speed are compared with those obtained with CMsin and CMsqr. The capacitor voltages at 30 r/min (1% of the rated speed) are shown in Fig. 7(a). The three techniques exhibit acceptable values of voltage ripple, with a maximum peak-to-peak value of 10 V for the CMsin, whereas CMsqr and DPWM present lower voltage ripple, with a peak-to-peak value of 7.5 V each.

Fig. 7(b) shows the reference and the measured circulating current values in red and blue colors, respectively. As defined in (3), the circulating current reference in DPWM consists of the product between the modulation index and the output current. The circulating current references contain a dc component plus some sinusoidal components. It can be demonstrated that the sinusoidal components are canceled among the three phases of the converter and do not appear in the dc-link current.

Whereas the capacitor voltage ripples with DPWM and CMsqr are very similar, the rms values of the circulating currents are not. CMsin produces higher circulating currents, with a peak value of 3 A and an rms value of 1.47 A. As expected from [25], CMsqr requires a smaller circulating current, with a measured peak value of 2.3 A, but a reference of 1.7 A, and an rms value of 1.17 A. Finally, DPWM produces the lowest circulating currents. Although the peak value of its current reference is 0.85 A, it has a measured peak value of 2.4 A. These peaks are caused by the capacitor voltage ripples. Since the capacitor voltages are not at their reference value, the voltage applied to the arm inductors during the clamping transitions changes suddenly, causing a pulse in the circulating current. Nevertheless, the duration of the current peaks is very short and they do not affect much the rms value of the circulating current, which is only 0.85 A, 30% less than that with CMsqr. As a result, DPWM also reduces the conduction losses of the converter when compared to CMsqr and CMsin.

Fig. 7(c) shows the PMSM currents using the low-frequency techniques. In all of them, some distortion appears but it is more significant in the cases of CMsin and CMsqr, both of which present a superimposed high-frequency ripple. However, in motor drive applications, the presence of these small glitches when using DPWM is not critical.

In order to demonstrate the power losses reduction of the DPWM technique, the efficiency of the different techniques has been measured. Fig. 8 shows the efficiency of the converter when using the four techniques studied in the speed range from 30 r/min to 150 r/min (CB-SVPWM has only been tested from 120 r/min to 150 r/min, as the size of the capacitor voltage oscillations makes it of no use at lower speeds). In all the cases, the same load torque has been applied. The efficiency values have been measured with a YOKOGAWA WT1600 Digital Power Meter.

Fig. 8 demonstrates that DPWM is the most efficient low-speed modulation technique, with efficiency values ranging from 76% to 85%. On the contrary, CMsin is the least efficient one, with efficiency values from 54% at 30 r/min to 69% at 150 r/min. Even in case of using CMsin or CMsqr with no additional SMs (CMsin-1 or CMsqr-1), their efficiency is worse. The reduction in power losses with DPWM is mostly due to the reduction in the circulating current values, and therefore, in the conduction losses. The switching power losses do not play an important role in this analysis since the MMC prototype is made of SiC devices, which have very small switching losses. For this reason, in the operation points where CB-SVPWM can be applied, i.e., medium and high speeds, CB-SVPWM is the most efficient one, since it requires lower circulating currents, provided that the converter uses SiC transistors. However, when the converter is made with Si switches, DPWM will be more efficient than CB-SVPWM even for medium and high speeds. Fig. 9 depicts phase-to-phase output voltage THD and WTHD, at different motor speeds, for different modulation techniques and with or without an additional SM. As the output voltage frequency varies with the motor speed, all the harmonics up to 12,500 Hz have been computed in order to cover at least twice the switching frequency in all the cases. In terms of THD, DPWM improves gradually with the motor speed. As for the WTHD, it can be noticed that the values obtained with DPWM are significantly better than the ones obtained with the other low speed techniques. As it was to be expected, removing the

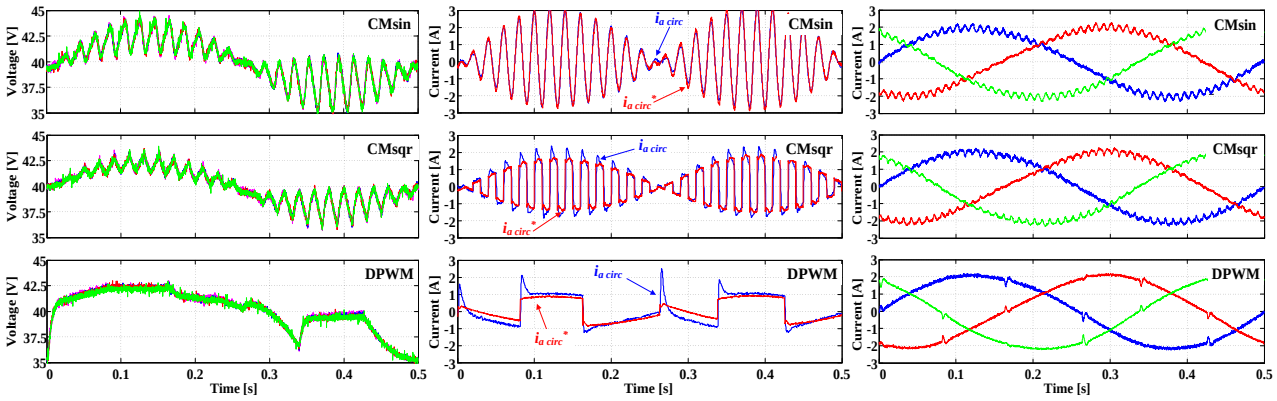

Fig. 7. Experimental results obtained at low speed (30 r/min). (a) Capacitor voltages, (b) reference and measured circulating current in phase-leg a, and (c) converter output currents.

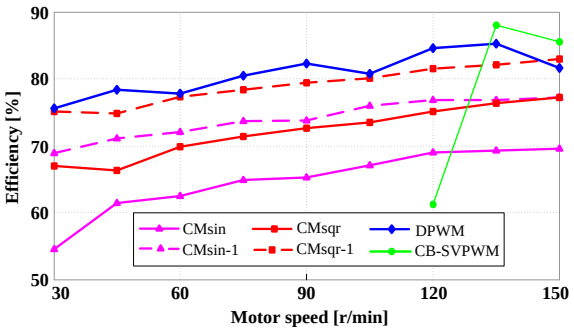

Fig. 8. Converter efficiency between 30 and 150 r/min.

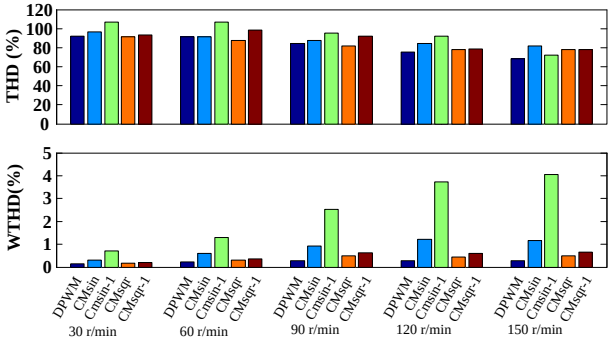

Fig. 9. Output voltage THD and WTHD for different motor speeds.

extra SMs renders worse WTHD values for all the studied modulation techniques.

D. Speed Range and Dynamic Performance

The speed range of CMsin and CMsqr is limited, since they are based on the injection of a zero-sequence voltage that is not naturally adapted to the speed regime of the electrical machine. When the rotational speed of the machine is close to the nominal speed and, consequently, the amplitude of the fundamental voltage is close to the rated voltage as well, there is a limitation on the maximum achievable zero-sequence voltage that can be used with CMsin and CMsqr. Otherwise the converter would enter into the over-modulation region. This fact forces to switch from one strategy to another or, alternatively, to modify adaptively the amplitude and frequency of the zero-sequence voltage as a function of the speed of the machine [21], [23], [26], [39], [40]. On the contrary, since the zero-sequence voltage in DPWM is calculated based on the instantaneous output currents and voltage reference signals, it is automatically adapted to the speed regime and there is no need to implement any mechanism to switch from a low-speed modulation technique to a medium- or high- speed modulation technique. This allows DPWM to perform very well at low and high speeds.

Fig. 10 shows the output currents of the converter when a reference step from 30 r/min to 1500 r/min (1% to 50% of the nominal speed) is applied to the speed controller. The dynamics of this speed change are not affected by the modulation technique, but only by the motor dynamics and the tuning of the FOC controllers. As can be seen, DPWM performs well within all the speed range.

V. Conclusion

In this paper, the discontinuous modulation technique has been applied to the MMC in a motor drive application. The discontinuous modulation has been adapted to be used in a PMSM drive, which includes the design of a new energy control for modulation techniques with high zero-sequence injection. The effectiveness of the proposed technique has been demonstrated with experimental results. Operation of the PMSM at low speeds has been tested and benchmarked against other low-speed techniques based on the injection of sinusoidal and square-wave zero-sequence signals. The results demonstrate the capability of discontinuous modulation to reduce the capacitor voltage ripples, allowing the PMSM to operate at very low speeds with capacitor voltage ripple amplitudes similar to those obtained with other state-of-the-art techniques. Moreover, when compared to the other low-speed techniques, the discontinuous modulation reduces the power losses and hence increases the converter efficiency.

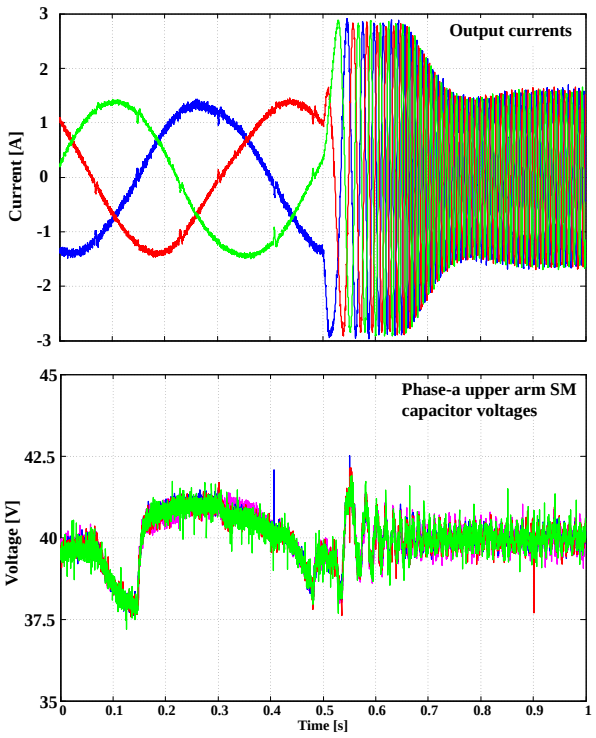

Fig. 10. Experimental results using DPWM and applying a step change from 30 r/min to 1500 r/min in the speed reference (1% to 50% of the nominal speed) at $t = 0.5$ s.

REFERENCES

[1] L.G. Franquelo, J. Rodriguez, J.I. Leon, S. Kouro, R. Portillo, and M.A.M. Prats, "The age of multilevel converters arrives," *IEEE Ind. Electron. Magazine*, vol. 2, no. 2, pp. 28–39, Jun. 2008.

[2] S. Kouro, M. Malinowski, K. Gopakumar, J. Pou, L.G. Franquelo, B. Wu, J. Rodriguez, M.A. Perez, and J.I. Leon, "Recent advances and industrial applications of multilevel converters," *IEEE Trans. Ind. Electron.*, vol. 57, no. 8, pp. 2553–2580, Aug. 2010.

[3] A. Lesnicar and R. Marquardt, "An innovative modular multilevel converter topology suitable for a wide power range," in *Proc. IEEE Power Tech Conf.*, Bologna, Italy, 23–26 Jun. 2003, vol. 3, pp. 272–277.

[4] S. Debnath, J. Qin, B. Bahrani, M. Saeedifard, and P. Barbosa, "Operation, control, and applications of the modular multilevel converter: a review," *IEEE Trans. Power Electron.*, vol. 30, no. 1, pp. 37–53, Mar. 2014.

[5] M.A. Perez, S. Bernet, J. Rodriguez, S. Kouro, and R. Lizana, "Circuit topologies, modelling, control schemes and applications of modular multilevel converters," *IEEE Trans. Power Electron.*, vol. 30, no. 1, pp. 4–17, Mar. 2014.

[6] M. Saeedifard and R. Iravani, "Dynamic performance of a modular multilevel back-to-back HVDC system," *IEEE Trans. Power Del.*, vol. 25, no. 4, pp. 2903–2912, Oct. 2010.

[7] H. P. Mohammadi and M. Tavakoli Bina, "A transformerless medium-voltage STATCOM topology based on extended modular multilevel converters," *IEEE Trans. Power Electron.*, vol. 26, no. 5, pp. 1534–1545, May 2011.

[8] M. Hagiwara, K. Nishimura, and H. Akagi, "A medium-voltage motor drive with a modular multilevel PWM inverter," *IEEE Trans. Power Electron.*, vol. 25, no. 7, pp.1786–1799, Jul. 2010.

[9] M. Hiller, D. Krug, R. Sommer, and S. Rohner, "A new highly modular medium voltage converter topology for industrial drive applications," in *Proc. EPE Conf. Appl.*, Barcelona, Spain, Sep. 8–10 2009, pp. 1–10.

[10] K. Wang, Y. Li, Z. Zheng, and L. Xu, "Voltage balancing and fluctuation-suppression methods of floating capacitors in a new modular multilevel converter," *IEEE Trans. Ind. Electron.*, vol. 60, no. 5, pp. 5063–5073, Nov. 2013.

[11] Y. S. Kumar and G. Poddar,"Control of medium-voltage AC motor drive for wide speed range using modular multilevel converter," *IEEE Trans. Ind. Electron.*, vol. 64, no. 4, pp. 2742-2749, Apr. 2017.

[12] B. Li, S. Zhou, D. Xu, S. J. Finney, and B. W. Williams, "A hybrid modular multilevel converter for medium-voltage variable-speed motor drives," *IEEE Trans. Power Electron.*, vol. 32, no. 6, pp. 4619–4630, Jun. 2017.

[13] B. Tai, C. Gao, X. Liu, and Z. Chen, "A novel flexible capacitor voltage control strategy for variable-speed drives with modular multilevel converters," *IEEE Trans. Power Electron.*, vol. 32, no. 1, pp. 128–141, Jan. 2017.

[14] W. Kawamura, K.-L. Chen, M. Hagiwara, and H. Akagi, "A low-speed, high-torque motor drive using a modular multilevel cascade converter based on triple-star bridge cells (MMCC-TSBC)," *IEEE Trans. Ind. Appl.*, vol. 51, no. 5, pp. 3965–3974, Sep./Oct. 2015.

[15] L. He, K. Zhang, J. Xiong, S. Fang, and Y. Xue, "Low-frequency ripple suppression for medium-voltage drives using modular multilevel converter with full-bridge submodules," *IEEE J. Emerg. Sel. Topics Power Electron.*, vol. 4, no. 2, pp. 657–667, Jun. 2016.

[16] S.P. Engel and R.W. De Doncker, "Control of the modular multi-level converter for minimized cell capacitance," in *Proc. EPE Conf. Appl.*, Birmingham, UK, Aug. 30–Set. 1 2011, pp. 1–10.

[17] K. Ilves, S. Norrga, L. Harnefors, and H.-P. Nee, "On energy storage requirements in modular multilevel converters, *IEEE Trans. Power Electron.*, vol. 29, no. 1, pp. 77–88, Jan. 2014.

[18] J. Pou, S. Ceballos, G. Konstantinou, V.G. Agelidis, R. Picas, and J. Zaragoza, "Circulating current injection methods based on instantaneous information for the modular multilevel converter," *IEEE Trans. Ind. Electron.*, vol. 62, no. 2, pp. 777–788, Feb. 2015.

[19] R. Yang, B. Li, G. Wang, C. Cecati, S. Zhou, and D. Xu, "Asymmetric mode control of MMC to suppress capacitor voltage ripples in low-frequency, low-voltage conditions, *IEEE Trans. Power Electron.*, vol. 32, no. 6, pp. 4219–4230, Jun. 2017.

[20] B. Li, S. Zhou, D. Xu, R. Yang, C. Buccella, and C. Cecati, "An improved circulating current injection method for modular multilevel converters in variable-speed drives," *IEEE Trans. Ind. Electron.*, vol. 63, no. 11, pp. 7215–7225, Nov. 2016.

[21] A.J. Korn, M. Winkelnkemper, and P. Steimer, "Low output frequency operation of the modular multi-level converter," in *Proc. IEEE Energy Conversion Congress and Exposition (ECCE)*, Atlanta, USA, Set. 12–16 2010, pp. 3993–3997.

[22] J. Kolb, F. Kammerer, M. Gommeringer, and M. Braun, "Cascaded control system of the modular multilevel converter for feeding variable-speed drives," *IEEE Trans. Power Electron.*, vol. 30, no. 1, pp. 349–357, Jan. 2015.

[23] A. Antonopoulos, L. Ängquist, S. Norrga, K. Ilves, L. Harnefors, and H.-P. Nee, "Modular multilevel converter AC motor drives with constant torque from zero to nominal speed," *IEEE Trans. Ind. Appl.*, vol. 50, no. 3, pp. 1982–1993, May/Jun. 2014.

[24] A. Antonopoulos, L. Ängquist, L. Harnefors, and H.-P. Nee, "Optimal selection of the average capacitor voltage for variable-speed drives with modular multilevel converters," *IEEE Trans. Power Electron.*, vol. 30, no. 1, pp. 227–234, Jan. 2015.

[25] M. Hagiwara, I. Hasegawa, and H. Akagi, "Start-up and low-speed operation of an electric motor driven by a modular multilevel cascade inverter," *IEEE Trans. Ind. Appl.*, vol. 49, no. 4, pp. 1556-1565, Jul./Aug. 2013.

[26] J.-J. Jung, H.-J. Lee, and S.-K. Sul, "Control strategy for improved dynamic performance of variable-speed drives with modular multilevel converter," *IEEE J. Emerg. Sel. Topics Power Electron.*, vol. 3, no. 2, pp. 371–380, Jun. 2015.

[27] S. Debnath, J. Qin, and M. Saeedifard, "Control and stability analysis of modular multilevel converter under low-frequency operation," *IEEE Trans. Ind. Electron.*, vol. 62, no. 9, pp. 5329–5339, Sep. 2015.

[28] R. Picas, S. Ceballos, J. Pou, J. Zaragoza, G. Konstantinou, and V.G. Agelidis, "Improving capacitor voltage ripples and power losses of modular multilevel converter through discontinuous modulation," in *Proc. IEEE Ind. Electron. Conf. (IECON)*, Vienna, Austria, 10–13 Nov. 2013, pp. 6233–6238.

[29] R. Picas, S. Ceballos, J. Pou, J. Zaragoza, G. Konstantinou, and V.G. Agelidis, "Closed loop discontinuous modulation technique for capacitor voltage ripples and switching losses reduction in modular multilevel converters," *IEEE Trans. Power Electron.*, vol. 30, no. 9, pp. 4714–4725, Sep. 2015.

[30] A. Antonopoulos, L. Ängquist, and H.-P. Nee, "On dynamics and voltage control of the modular multilevel converter," in *Proc. EPE Conf. Appl.*, Barcelona, Spain, 8–10 Set. 2009, pp 1-10.

[31] V.G. Agelidis, P.D. Ziogas, and G. Joos, "Dead-band PWM switching patterns," *IEEE Trans. Power Electron.*, vol.11, no.4, pp. 522–531, Jul. 1996.
[32] G. Konstantinou, J. Pou, S. Ceballos, and V.G. Agelidis, "Active redundant submodule configuration in modular multilevel converters," *IEEE Tran. Power Del.*, vol. 28, no. 4, pp. 2333–2341, Oct. 2013.
[33] R. Picas, S. Ceballos, J. Pou, J. Zaragoza, G. Konstantinou, V. G. Agelidis, and J. Balcells "Discontinuous modulation of modular multilevel converters without the need for extra submodules" in *Proc. IEEE Ind. Electron. Conf. (IECON)*, Yokohama, Japan, 9–12 Nov. 2015, pp. 2538–2543.
[34] S. Ceballos, J. Pou, S Choi, M. Saeedifard, and V. Agelidis, "Analysis of voltage balancing limits in modular multilevel converters," in *Proc. IEEE Ind. Electron. Conf. (IECON)*, Melbourne, Australia, 7–10 Nov. 2011, pp. 4397–4402.
[35] A. Hassanpoor, S. Norrga, H. P. Nee, and L. Ängquist, "Evaluation of different carrier-based PWM methods for modular multilevel converters for HVDC application, in *Proc. Int. IEEE Ind. Electron. Conf. (IECON)*, Montreal, QC, Canada, 25–28 Oct. 2012, pp. 388–393.
[36] R. Darus, G. Konstantinou, J. Pou, S. Ceballos, and V. G. Agelidis, "Comparison of phase-shifted and level-shifted PWM in the modular multilevel converter," in *Proc. Int. Power Electron Conf. (IPEC)*, Hiroshima, Japan,18–21 May 2014, pp. 3764–3770.
[37] R. Darus, J. Pou, G. Konstantinou, S. Ceballos, R. Picas, and V.G. Agelidis, "A modified voltage balancing algorithm for the modular multilevel converter: evaluation for staircase and phase-disposition PWM," *IEEE Trans. Power Electron.*, vol. 30, no. 8, pp. 4119–4127, Aug. 2015.
[38] B.K. Bose, "Modern power electronics and ac drive," *Prentice Hall PTR*, 2001.
[39] Y. Okazaki, M. Hagiwara, and H. Akagi, "A speed-sensorless start-up method of an induction motor driven by a modular multilevel cascade inverter (MMCI-DSCC)," *IEEE Trans. Ind. Appl.*, vol. 50, no. 4, pp. 2671–2680, Jul./Aug. 2014.
[40] M. Hagiwara, I. Hasegawa, and H. Akagi, "Startup and Low-Speed Operation of an Adjustable-Speed Motor Driven by a Modular Multilevel Cascade Inverter (MMCI)," in *Proc. IEEE Energy Conversion Congress and Exposition (ECCE)*, Raleigh, USA, 15–20 Sep. 2015, pp. 718–725.

Ricard Picas received the B.S., the M.S. and the Ph.D. degree in electronics engineering, from the Technical University of Catalonia (UPC), Spain, in 2010, 2012, and 2016, respectively.

From September 2012 to October 2016 he was a Predoctoral Researcher with the Terrassa Industrial Electronics Group, UPC. From January 2016 to June 2016 he was a Visiting Researcher at the Power Electronics, Machines and Control Group (PEMC), University of Nottingham, UK. Since November 2016 he has been with Ingenia Motion Control, Barcelona, Spain. His main research interests include multilevel converters, power conversion efficiency and wide bandgap semiconductors.

Jordi Zaragoza (S'08-M'12) received the B.S., M.S. and Ph.D. degrees from the Technical University of Catalonia (UPC), Spain, in 2001, 2004, and 2011 respectively.

In 2003, he joined the faculty of UPC as an Assistant Professor and became an Associate Professor in 2012. From September 2006 to September 2007 he was a researcher at the Energy Unit of ROBOTIKER-TECNALIA Technologic Corporation, Basque Country, Spain. He has been involved in several projects in the fields of power electronics and systems. His research interests include modeling and control of power converters, multilevel converters, wind energy, power quality and HVDC transmission systems.

Josep Pou (S'97–M'03–SM'13–F'17) received the B.S., M.S., and Ph.D. degrees in electrical engineering from the Technical University of Catalonia (UPC), Spain, in 1989, 1996, and 2002, respectively.

In 1990, he joined the faculty of UPC as an Assistant Professor, where he became an Associate Professor in 1993. From February 2013 to August 2016, he was a Full Professor with the University of New South Wales (UNSW), Sydney, Australia. He is currently an Associate Professor with the Nanyang Technological University, Singapore. In 2001 and 2005, he was a Researcher at the Center for Power Electronics Systems, Virginia Tech, Blacksburg. In 2012, he was a Visiting Professor at the Australian Energy Research Institute, UNSW, Sydney. His research interests include power electronics, multilevel converters, renewable energy, energy storage, power quality, HVDC transmission systems, and more-electrical aircraft and vessels.

Salvador Ceballos received the M.S. degree in physics from the University of Cantabria, Santander, Spain, in 2001, and the M.S. and Ph.D. degrees in electronic engineering from the University of the Basque Country, Bilbao, Spain, in 2002 and 2008, respectively.

Since 2002, he has been with Tecnalia Research and Innovation, Derio, Spain., where he is currently a Researcher at the Energy and Environmental Division. From May 2008 to May 2009, he was a Visiting Researcher with the Hydraulic and Maritime Research Centre, University College Cork, Cork, Ireland. From November 2014 to May 2015, he was a Visiting Researcher with the Australian Energy Research Institute, University of New South Wales, Sydney, Australia. His research interests include multilevel and fault-tolerant power electronic converters, and renewable energy systems.

Georgios Konstantinou (S'08–M'11–SM'18) received the B.Eng. degree in electrical and computer engineering from the Aristotle University of Thessaloniki, Thessaloniki, Greece, in 2007 and the Ph.D. degree in electrical engineering from UNSW Sydney (The University of New South Wales), Australia, in 2012.

From 2012 to 2015 he was a Research Associate at UNSW. He is currently a Lecturer with the School of Electrical Engineering and Telecommunications at UNSW and an Australian Research Council (ARC) Early Career Research Fellow. His main research interests include hybrid and modular multilevel converters, power electronics for HVDC and energy storage applications, pulse width modulation and selective harmonic elimination techniques for power electronics. Dr. Konstantinou is an Associate Editor of IEEE Transactions on Power Electronics and IET Power Electronics.

Gabriel J. Capella received the B.S, M.S. and Ph.D. degrees in electrical engineering from the Technical University of Catalonia (UPC), Spain, in 1985, 2001 and 2015, respectively.

Since 1986 he has been with the UPC where he is currently an Associate Professor. His research interests include parallel-connected converters, power quality, renewable energy systems and fault tolerant power electronics systems.